Generation of dense electron-hole plasmas in silicon

K. Sokolowski-Tinten and D. von der Linde
Institut für Laser- und Plasmaphysik, Universität-GHS-Essen, D-45117 Essen, Federal Republic of Germany
(Received 20 November 1998; revised manuscript received 7 July 1999)

Generation of dense electron-hole plasmas in silicon with intense 100-fs laser pulses is studied by time-resolved measurements of the optical reflectivity at 625 nm. For fluences F between 10 mJ/cm$^2 < F < 400$ mJ/cm^2, plasma generation is dominated by strong two-photon absorption, and possibly higher-order nonlinearities, which lead to very steep spatial carrier distributions. The maximum carrier densities at the sample surface are in excess of 10^{22} cm^{-3}, and therefore, the reflectivity shows a mainly Drude-like free-carrier response. Within the Drude model, limits for the optical effective mass and the damping time are determined.

I. INTRODUCTION

The properties of optically excited electron-hole plasmas in semiconductors have been extensively studied during the past two decades.[1] The availability of femtosecond laser pulses has led to an enormous progress, because the electronic properties of semiconductors are determined by the basic relaxation processes of the free carriers, which occur in the subpicosecond time domain. In most cases, the experimental work was limited to carrier densities below 10^{20} cm^{-3}.

Work on electron-hole plasmas of higher density has been done in connection with the investigation of nanosecond and picosecond laser-induced phase transitions in solid materials. Starting with the discovery of laser annealing[2] of crystal damage in ion-implanted semiconductors at the end of the 1970s and the attempts by Van Vechten *et al.*[3] to explain these processes by the so-called *plasma model*, there was a controversial debate[4] about the mechanisms of melting by short laser pulses. This stimulated a great deal of experimental[5–10] and theoretical[11–14] work on the properties of laser excited *e-h* plasmas up to the 10^{21}-cm^{-3} range. Meanwhile, it was generally accepted[15] that for pulse durations down to a few picoseconds the phase transformation is a rapid thermal process, due to the fast energy exchange between the optically excited electronic subsystem and the lattice.

The situation is quite different when much shorter laser pulses are used. Time-resolved optical experiments on femtosecond excited silicon,[16–18] gallium arsenide,[18–21] indium antimonide,[22] and carbon[23] gave strong evidence that the transition to the disordered liquid phase is possible on a subpicosecond time scale, too fast to be explained by thermal processes. Based on Van Vechten and co-workers' idea[3,24] of plasma-induced softening of the crystal lattice, a number of theoretical studies[25–29] investigated nonthermal melting in semiconductors. These studies set a lower density limit of approximately 10^{22} cm^{-3} for the proposed lattice instability. However, only few experiments[30–33] directly addressed this density range. The experimental verification of densities in excess of 10^{22} cm^{-3}, and a thorough understanding of the properties of such dense *e-h* plasmas, is still lacking.

In a recent paper[18] we presented a detailed investigation of femtosecond laser-induced melting in silicon and gallium arsenide by means of time-resolved measurements of the optical reflectivity and the reflected second harmonic. These experiments provided changes of the linear optical constants and of the second-order nonlinear optical susceptibility. Our data suggest a simple two-step model of the laser-induced phase transition. This model distinguishes between an *excitation stage* and a *transition stage*. While Ref. 18 emphasized the melting process during the transition stage, the present paper will focus on the excitation stage. We have investigated in detail the carrier generation processes and the plasma properties in silicon at very early times before melting occurs.

The paper is organized as follows. In Sec. II we briefly describe the experimental setup. Based on results from previous work on low-density *e-h* plasmas, Sec. III discusses the expected laser-induced changes of the optical properties. In Sec. IV we describe and analyze the experimental data. As the main result, a lower limit of the density of the *e-h* plasma as a function of excitation fluence is derived, giving *quantitative* evidence for *e-h* densities in excess of 10^{22} cm^{-3}. A summary and some conclusions concerning the relevance of the results in the context of femtosecond laser induced melting are presented in Sec. V.

II. EXPERIMENT

To investigate the generation and the properties of dense electron-hole plasmas in silicon, time-resolved measurements of the reflectivity have been performed on single-crystalline,[34] optically polished samples. We applied standard femtosecond pump-probe techniques using 100-fs light pulses at 625 nm provided by a 10-Hz-amplified colliding-pulse, passively mode-locked dye-laser (rhodamine6G/DODCI). The *s*-polarized pump beam struck the sample surface at an angle of incidence of 30°; the probe beam was *p* polarized with an angle of incidence of 49°. The probe was focused to the central part of the excited area to minimize the effects of spatial averaging. The silicon wafers were raster scanned during the measurements by a stepper-motor-driven two-axis translation stage in order to ensure that each pump pulse strikes a fresh, unexcited area on the sample surface.

For each laser shot the energy of the pump and the probe beam and the reflectivity were measured by calibrated *p-i-n* photodiodes. Great care was taken to measure the excitation fluence precisely. We used a diode array in a reference plane representing a replica of the target surface to control the spatial intensity distribution of the pump beam on the sample. During the experimental runs the diode array was replaced by a suitable pinhole followed by an additional photodiode. The pinhole represents that part of the excited area which is actually interrogated by the probe beam. Due to small pulse-to-pulse variations of the beam profile of the focused pump beam and variations of the spatial overlap between pump and probe, the local pump fluence turned out to be a much better energy reference than the total pump energy. By this technique the scattering of the measured reflectivity data could be significantly reduced.

The fluence of the excitation pulse was varied from below 0.01 J/cm^2 up to 0.4 J/cm^2 with the help of a half-wave plate in conjunction with an optical polarizer. The highest fluence corresponds to approximately 2.5 times the melting threshold of 0.17 J/cm^2. The fluence of the probe pulse was kept at a level of about a few hundred μJ/cm^2, well below the single-shot melting threshold.

III. OPTICAL PROPERTIES OF STRONGLY EXCITED SILICON

This section discusses the electronic structure of strongly excited silicon, and the expected changes of the optical properties. We are dealing with electron-hole densities around 10^{22} cm^{-3}. The temperature of the plasma could be roughly estimated from the effective excess energy of the electron-hole pairs, which is greater than the single-photon excess energy $\hbar\omega_0 - E_{gap}$. As we show later, this is due to the strong two-photon[32,33] and free-carrier contributions to the overall absorption of the pump pulse. The initial distribution of the excited *e-h* pairs thermalizes very rapidly within a few tens of femtoseconds[35,36] due to ultrafast carrier-carrier scattering. Thus the initial carrier temperature should be above 10^4 K, making the plasma nondegenerate even at these high densities.[37]

To deduce some basic guidelines concerning the expected changes of the optical properties, we extrapolate the results of previous low-excitation work to the density and temperature regimes encountered in this study. Three physical effects are responsible for changes of the linear optical properties of a semiconductor: (i) state and band filling,[39,40] (ii) renormalization of the band structure,[41] and (iii) the free-carrier response. For simplicity we assume first that each mechanism contributes separately to the dielectric constant ϵ^* of the excited material:

$$\epsilon^* = \epsilon_g + \Delta\epsilon_{pop} + \Delta\epsilon_{bgs} + \Delta\epsilon_{fcr}. \tag{1}$$

Here ϵ_g is the dielectric constant of the unexcited material [Si, 625 nm (Ref. 42): $\epsilon_g = 15.26 + i0.17$]. $\Delta\epsilon_{pop}$, $\Delta\epsilon_{bgs}$, and $\Delta\epsilon_{fcr}$ represent the changes of the dielectric constant due to state and band filling, renormalization of the band structure, and the free-carrier response, respectively.

A. State and band filling

A description of the effect of state and band filling ($\Delta\epsilon_{pop}$) would, in principle, require a detailed knowledge of the carrier distribution in the conduction and valence bands. However, due to the high plasma temperature it is reasonable to assume that the carriers are almost uniformly distributed over the Brillouin zone. Therefore, no distinct spectral structures such as spectral hole burning[39] would be expected, and the magnitude of $\Delta\epsilon_{pop}$ could be simply estimated from the ratio of the density $N_{e\text{-}h}$ of excited *e-h* pairs and the total valence-band density N_0 (silicon: $N_0 = 2\times10^{23}$ cm^{-3}) in the unexcited state:[25]

$$\Delta\epsilon_{pop} = -(\epsilon_g - 1)\frac{N_{e\text{-}h}}{N_0}. \tag{2}$$

B. Band-structure renormalization

Band-structure renormalization describes changes of the single-particle energy of the carriers due to many-body interactions in the excited plasma. Often these changes are treated as a rigid shift of the band structure resulting in a shrinkage of the energy gap (ΔE_{gap}) which is proportional to the cubic root of the density.[41,43,44] Deviations from the simple cubic root law are expected due to the temperature dependence of ΔE_{gap},[45] and additional high density contributions described by Kim and co-workers.[46] Neglecting the latter effects the changes of the optical properties can be estimated within the rigid band shift model from a corresponding shift of the optical spectra:[33]

$$\Delta\epsilon_{bgs} = \epsilon_g(\hbar\omega + \Delta E_{gap}) - \epsilon_g(\hbar\omega). \tag{3}$$

C. Free-carrier response

The changes of the optical constants caused by the response of the free carriers can be described by the Drude model[47]

$$\Delta\epsilon_{fcr} = -\frac{N_{e\text{-}h}e^2}{\epsilon_0 m^*_{opt} m_e \omega^2}\frac{1}{1+i\dfrac{1}{\omega\tau_D}} = -\left(\frac{\omega_P}{\omega}\right)^2\frac{1}{1+i\dfrac{1}{\omega\tau_D}}, \tag{4}$$

where ϵ_0, m_e, and ω have their usual meanings, $m^*_{opt} = (m_e^{*-1} + m_h^{*-1})^{-1}$ denotes the optical effective mass of the carriers (m_e^* and m_h^* are the mobility effective masses of electrons and holes), τ_D the Drude damping time, and $\omega_P = \sqrt{N_{e\text{-}h}e^2/\epsilon_0 m^*_{opt} m_e}$ is the *plasma frequency*.

The optical mass in silicon is known only for low-density, relaxed plasmas, where the carriers occupy states near the band edges. Using common definitions for the mobility effective masses[48] and tabulated values for the different mass parameters in silicon,[50] a value of $m^*_{opt} = 0.15$ is found. Considering again the high density and high temperature of the *e-h* plasma with carriers far from the band edges, the assumption of a constant mass parameter is questionable, because of the nonparabolicity of the bands. Under these conditions the optical mass in Eq. (3) must be calculated as an average over all occupied states,[51] which again requires a

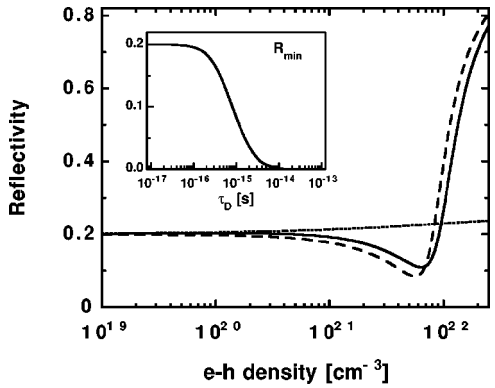

FIG. 1. Theoretical predictions for the reflectivity of silicon as a function of the excited electron-hole density, 625-nm wavelength, 49° angle of incidence, and *p* polarization. Dotted curve: contributions due to state and band filling and band-gap shrinkage; dashed curve: pure Drude contribution; solid curve: total reflectivity according to Eq. (5). Inset: minimal reflectivity as a function of the Drude damping time.

knowledge of the carrier distribution functions; m^*_{opt} will become in principle a density- and temperature-dependent quantity.[12,13]

Similar restrictions apply for the Drude damping time τ_D which also becomes density and temperature dependent.[52,53] At low densities the current relaxation is determined by carrier-phonon collisions ($1/\tau_D \approx 10^{13}$ s^{-1}). For higher densities carrier-carrier collisions, in which the total momentum, but not the current, is conserved, are thought to be responsible for the high damping rates ($1/\tau_D \approx 10^{15}$ s^{-1}) observed in previous high-density experiments.[5,31]

Although no detailed experimental data exist on the density and temperature dependences of the Drude parameters, it will be shown in Sec. IV that the changes of the optical properties are dominated by the response of the free carriers at the high densities we are dealing with in this work.

D. Optical constants and reflectivity

Summarizing the discussion of the last paragraphs the following expression for the dielectric function of an optically excited semiconductor can be derived:

$$\epsilon^*(\hbar\omega) = 1 + [\epsilon_g(\hbar\omega + \Delta E_{gap}) - 1]\frac{N_0 - N_{e\text{-}h}}{N_0} - \frac{N_{e\text{-}h}e^2}{\epsilon_0 m^*_{opt} m_e \omega^2}\frac{1}{1 + i\dfrac{1}{\omega\tau_D}}. \quad (5)$$

We will use this equation to analyze in more detail the expected changes of the reflectivity and the importance of the different contributions. For simplicity we assume a temperature-independent gap shrinkage and constant values for the optical mass and the damping time. For the last two parameters we choose $m^*_{opt} = 0.18$ and $\tau_D = 1$ fs (see experimental data). In Fig. 1 the *p*-polarized reflectivity of silicon for $\lambda = 625$ nm at an angle of incidence of 49° is plotted as a function of the carrier density.

The dotted curve represents the combined contributions due to state and band filling and band-gap renormalization according to the first part of Eq. (5). Due to the opposite sign of the two effects the change in reflectivity is relatively small. The dashed curve shows the reflectivity derived from a pure Drude model [the free-carrier response alone; see Eq. (4)]. Very briefly, the main reflectivity features of the pure Drude model are the decrease at lower densities and a drastic increase at higher densities. The reflectivity minimum corresponds to the density where the real part of ϵ^* is equal to 1. The reflectivity increases when the electron-hole density exceeds the *critical density* N_{cr} which corresponds to $\mathrm{Re}(\epsilon^*) = 0$ [also called the *plasma resonance*: $\omega_P \approx \sqrt{\mathrm{Re}(\epsilon_g)}\omega$]. With the given optical constants and the chosen Drude parameters ($m^*_{opt} = 0.18$, $\tau_D = 1$ fs) the value of the critical density is $N_{cr} = 8.7 \times 10^{21}$ cm^{-3}. The value of the reflectivity at the minimum and the slope of the rising part are determined by the magnitude of the imaginary part of ϵ^*, which depends (in the pure Drude model) only on the damping constant. The inset of Fig. 1 shows the minimum reflectivity as function of the Drude damping time τ_D. For a strongly damped plasma ($\omega\tau_D \ll 1$) the minimum reflectivity stays close to the value of the unperturbed solid; for a weakly damped plasma ($\omega\tau_D \gg 1$), it approaches zero.

The solid curve represents the reflectivity calculated with the total dielectric function given in Eq. (5). The principal shape of this curve is very similar to the pure Drude model. This demonstrates that, especially at higher densities, free carriers dominate the optical response. Only for densities well below the critical density may the positive contribution resulting from gap shrinkage be stronger. Other differences between the dashed and solid curves are a slight increase of the critical density [caused by the increase of $\mathrm{Re}(\epsilon^*)$ due to gap shrinkage] and an increased reflectivity value at the minimum [due to the increase of $\mathrm{Im}(\epsilon^*)$]. Nevertheless, it is important to note that under high-density conditions the pure Drude model alone may be sufficient to interpret experimental reflectivity data: (i) The relation between carrier density and laser fluence is usually unknown. This relation determines position and slope of the plasma resonance (as a function of fluence). (ii) An increased damping constant can account for the changes of the minimum reflectivity.

IV. EXPERIMENTAL RESULTS AND ANALYSIS

In this section we describe the investigation of plasma generation and plasma properties in femtosecond photoexcited silicon. Experimentally, we measure the optical reflectivity of the probe pulse as a function of the pump pulse fluence. Such reflectivity data for four different delay times between pump and probe are shown in Fig. 2. Each data point represents the measured reflectivity of a *single* laser pulse. Due to the procedure described above of measuring the pump fluence on the actually probed portion of the excited area, no averaging of the data is necessary to obtain a high accuracy.

A. Melting dynamics

The results shown in Fig. 2 extend over a fluence range from below the melting threshold $F_m = 0.17$ J/cm^2 up to ap-

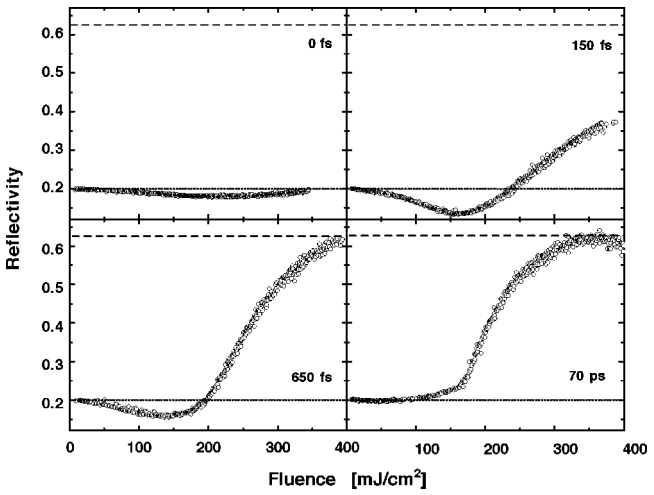

FIG. 2. Reflectivity of silicon as a function of excitation fluence for four different delay times, 625-nm wavelength, 49° angle of incidence, and *p* polarization. The dotted and dashed lines mark the reflectivity of solid and liquid silicon, respectively.

proximately $2.5\times F_m$. Although here we do not discuss in detail the solid-liquid phase transition (for details see, e.g., Refs. 18 and 21), it may be useful to give a brief description of the melting dynamics and the corresponding reflectivity changes. Upon melting, a drastic increase of the reflectivity due to the transformation from the semiconducting solid phase to the metallic liquid is expected (Fig. 2: dotted line R_{sol}, dashed line R_{liq}), in agreement with the general behavior of the measured curves. From a closer inspection of the data, different fluence regimes could be distinguished.

For fluences below F_m only relatively small changes of the reflectivity are observed. In this fluence regime the measured signals at early times are determined by the creation and relaxation of an electron-hole plasma, and, after approximately 1 ps, by the time evolution of the lattice temperature. We define the melting threshold as the lowest pump fluence for which the observed reflectivity rise equals the expected reflectivity of solid silicon at the equilibrium melting temperature of 1685° K.[54] Such a definition with reference to thermal melting is justified, because this reflectivity rise occurs rather slowly in tens of picoseconds (Fig. 2, $\Delta t = 70$ ps).

For fluences above F_m, melting must be taken into account. For gallium arsenide, it has been shown[18,56] that two different regimes of femtosecond laser-induced melting exist. In the vicinity of the melting threshold the solid-liquid phase transition is a slow, thermal process occurring on a 10–100 ps time scale. For higher fluences the experimental data show melting on a subpicosecond time scale. In this fluence regime melting is due to the plasma-induced lattice instability discussed in the introduction. The behavior observed on silicon is very similar (compare Fig. 2, $\Delta t = 650$ fs and $\Delta t = 70$ ps).

It should be noted, however, that a clear distinction between the highly excited solid phase and the molten phase is quite difficult.[18] For example, the shape of the reflectivity curves measured at $\Delta t = 150$ and 650 fs is in both cases in agreement with the behavior expected from the Drude model (Fig. 1). Nevertheless, the large increase of reflectivity observed for higher fluences at $\Delta t = 650$ fs occurs significantly *after* the pulse, and is related to the phase transition. As we have shown previously,[18] there is only a small time window just after the excitation pulse in which the strongly excited state of the solid phase can be studied. The following analysis will focus on the reflectivity data measured at very early times, e.g., $\Delta t = 150$ fs. At $\Delta t = 150$ fs creation of the *e-h* plasma is complete, but for most of the fluence range under investigation there is not enough time for relaxation of the plasma or melting. Only at the highest fluences shown here will the reflectivity be influenced by the very fast onset of nonthermal melting.[18] Therefore, the main conclusions of the analysis presented in the next sections are based on the reflectivity behavior at lower fluences (up to ≈ 300 mJ/cm^2).

B. Plasma generation and plasma density

As mentioned above, the reflectivity curves observed at early delay times follow the behavior expected from the Drude model. This shows that the free carriers dominate the optical response of the excited material, in agreement with the analysis presented in Sec. IV A. Before the Drude model is used to analyze our reflectivity data at $\Delta t = 150$ fs, we will briefly discuss the absorption of light in solid silicon. The absorption processes determine the density, the temperature, and the spatial profile of the excited carrier plasma. In silicon, electron-hole pairs are created by linear and by two-photon absorption (TPA).[32] Neglecting recombination and diffusion during and shortly after excitation, carrier generation can be described by the following differential equations for the carrier density and the pump intensity:

$$\frac{\partial}{\partial z} I(z,t) = -[\alpha_0 + \alpha_{fca}(z,t) + \beta I(z,t)] I(z,t), \tag{6}$$

$$\frac{\partial}{\partial t} N(z,t) = \left[\alpha_0 + \frac{1}{2}\beta I(z,t)\right] \frac{I(z,t)}{\hbar\omega}. \tag{7}$$

Here z denotes the spatial coordinate perpendicular to the surface. α_0 and β describe linear and two-photon interband absorption, and intraband free-carrier absorption is included via a space- and time-dependent coefficient α_{fcr}. Assuming a Gaussian pulse shape $I_0 e^{-(t/t_0)^2}$, the density equation can be integrated in time. To calculate the fraction of the incident laser-pulse energy which is coupled into the material, we neglect changes of the reflectivity R during the pump pulse. This is justified by the reflectivity curve for $\Delta t = 0$ fs in Fig. 2, which shows only slight changes of R as a function of fluence.[57] Using $F_0 = \sqrt{\pi} t_0 I_0$ the following result is obtained for the carrier density at the sample surface as a function of the excitation fluence F_0 (Ref. 32):

$$N_{e\text{-}h} = F_0 \frac{(1-R)}{\hbar\omega}\left[\alpha_0 + \beta F_0 \frac{(1-R)}{2\sqrt{2\pi} t_0}\right]. \tag{8}$$

Introducing the optical effective mass m^*_{opt} on both sides of this equation, and dividing by F_0, gives

$$\frac{N_{e\text{-}h}}{m^*_{opt} F_0} = \frac{\alpha_0 (1-R)}{m^*_{opt}\hbar\omega} + \frac{\beta (1-R)^2}{2\sqrt{2\pi} m^*_{opt} t_0 \hbar\omega} F_0. \tag{9}$$

While the right-hand side of Eq. (9) represents a simple linear function in F_0, the quantity on the left can be inferred from the measured data. By applying the Drude model, the

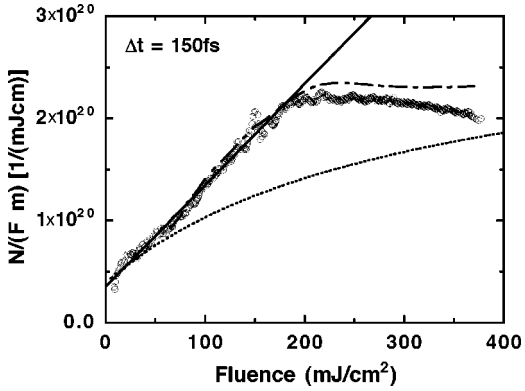

FIG. 3. Ratio $N_{e\text{-}h}/(m^*_{opt}F_0)$ as a function of laser fluence F_0. Open circles: measured data; solid line: linear fit to the data up to fluences of about 180 mJ/cm^2; dotted curve: numerical simulation under the assumption of a density-dependent optical mass; dash-dotted curve: back-calculated density from simulated reflectivity (solid curve in Fig. 6) neglecting the spatial inhomogeneity.

damping time τ_D can be determined from the minimum reflectivity R_{min}. The observed value of $R_{min}=13.5\%$ yields $\tau_D \approx 0.5$ fs. Knowing τ_D, the plasma density or, more precisely, the ratio $N_{e\text{-}h}/m^*_{opt}$, can be calculated from the measured reflectivity. The result is depicted in Fig. 3, where the experimentally determined ratio $N_{e\text{-}h}/(m^*_{opt}F_0)$ is plotted as a function of excitation fluence at $\Delta t = 150$ fs. The data follow the expected linear dependence up to fluences of about 180 mJ/cm^2 (solid curve: linear fit to the data; the dotted curve will be discussed below). With the help of Eq. (9), the parameters of the linear fit function can be used to extract the optical effective mass m^*_{opt} (intersection with ordinate) and the TPA coefficient β (slope). This yields $m^*_{opt}=(0.18 \pm^{0,04}_{0,02})$, in rather close agreement with the known value for low-density plasmas in silicon. A value of $\beta=(50\pm 10)$ cm/GW, somewhat higher than in previous studies,[32,33] is deduced. It must be concluded that in silicon TPA makes the dominant contribution to plasma generation: At the melting threshold of 170 mJ/cm^2, TPA is approximately one order of magnitude stronger than linear interband absorption [$\alpha_0 = 3.42\times 10^3$ cm^{-1},[42] and $\beta(1-R)I_0 \approx 3\times 10^4$ cm^{-1}].

Equation (9) can finally be used to infer from the measured data the absolute electron-hole densities. The result is shown by the data points in Fig. 4. The threshold density for nonthermal melting is approximately 10^{22} cm^{-3}. This limit is marked by the dashed line. The measured data clearly show that this density threshold is *exceeded.*

C. Spatial effects and model calculations

The dominance of TPA in the carrier generation process has important consequences. First, the excess energy of the created carriers and thus the plasma temperature is significantly increased. Second, the effective absorption length is much shorter than the linear absorption length ($1/\alpha_0 \approx 2$ μm). Therefore, TPA leads to very steep spatial carrier distributions. Under these conditions, the Fresnel formulas, which assume an optically homogeneous medium, are no longer properly describing the reflectivity. Instead, the distributed response of the spatial profile of the optical constants must be taken into account.

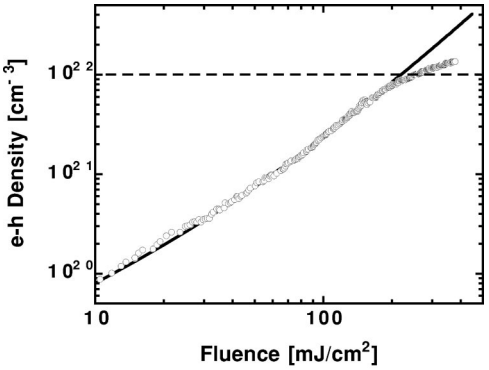

FIG. 4. Absolute electron-hole density as function of excitation fluence. Open circles: measured data points; solid curve: corrected density (taken from numerical simulations) to account for the steep spatial carrier distributions. The dashed line marks a *threshold* density of 10^{22} cm^{-3}.

To obtain an estimate on the influence of the spatial variation of the optical properties on the measured reflectivity data, we performed numerical calculations based on Eqs. (6) and (7), using the experimentally determined parameters (β, m^*_{opt}). Changes of the optical absorption are included via a space- and time-dependent dielectric function according to Eq. (5). As a result, the spatial carrier distributions as a function of time are obtained. As an example Fig. 5 shows the spatial carrier distributions 150 fs after the pump pulse for three selected pump fluences. The steepening of the carrier profiles with increasing fluence is evident. At 25 mJ/cm^2 the distribution is still exponential, although already with a decreased absorption depth due to TPA. At higher fluences the distributions develop a nonexponential shape with a drastically reduced effective absorption depth below 100 nm.

In a second step we used these carrier profiles to calculate the reflectivity of the probe pulse. To account for the spatial variation of the optical constants, we employed the matrix algorithm[58] of thin-film optics, which divides the profile into thin slices of constant optical properties. In this description, the distributed response is due to multiple interference at a large number of layers.

The reflectivity of a spatially nonhomogeneous *e-h* plasma still looks like a Drude response similar to Fig. 1.[8,30] Comparing with a homogeneous plasma, the main difference

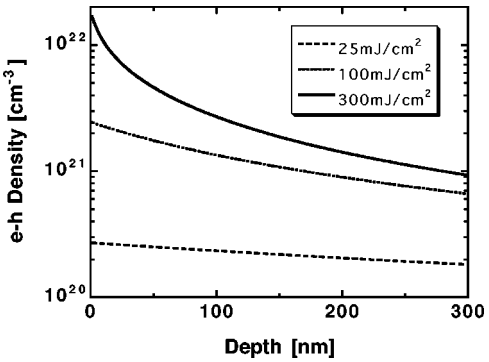

FIG. 5. Electron-hole density as a function of depth 150 fs after the pump pulse for three different pump fluences, as obtained from the numerical integration of Eqs. (6) and (7). Parameters of the calculation: $\beta=50$ cm/GW, $m^*_{opt}=0.18$, and $\tau_D=1.1$ fs (see text).

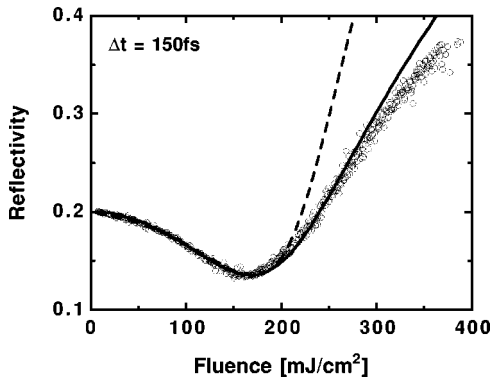

FIG. 6. Reflectivity of silicon as a function of laser fluence at a delay time of 150 fs. Open circles: measured data; dashed curve: numerical simulation using a homogeneous reflectivity model (Fresnel formula); solid line: numerical simulation taking into account the spatial variation of the optical properties.

is a flattening of the structures associated with the plasma resonance: (1) the minimum reflectivity value is raised, and (2) the slope of the reflectivity rise for higher densities is decreased. Qualitatively speaking, the spatial inhomogeneity has a similar effect as an increased damping (lower τ_D).

The latter point is demonstrated by Fig. 6, which shows the measured reflectivity data at $\Delta t = 150$ fs from Fig. 2 on an expanded scale. The dashed curve represents the reflectivity calculated from the results of our simulations using the Fresnel formula, where the spatial variation of the optical properties is ignored. It is assumed that the plasma density is constant, and corresponds to the maximum density at the sample surface as obtained from the simulation. The solid curve uses the same numerical results as before, but takes into account the spatial carrier profile. Both models provide a good approximation to the measured reflectivity up to fluences of about 180 mJ/cm^2. While the homogeneous description fails at higher excitation, a much better fit is obtained with the inhomogeneous model. For the homogeneous model, a shorter damping $\tau_D = 0.5$ fs is necessary, whereas for the inhomogeneous model we have $\tau_D = 1.1$ fs. In the density calculations the latter value was used to determine α_{fcr} in order to maintain self-consistency between the density- and the reflectivity-calculations.

The conclusions drawn from Fig. 6 justify the use of a homogeneous model (Fresnel formula) in the analysis of our reflectivity data for fluences below 180 mJ/cm^2. It is sufficient to adjust the damping constant to account for the spatial variation of the *e-h* density. This explains why below 180 mJ/cm^2, Eq. (9), which was derived for the carrier density at the *sample surface*, gives such a good approximation of the measured data. Moreover, it becomes quite clear why there are deviations from the linear dependence in Fig. 3 at higher fluences. These deviations are not due to changes of material parameters (i.e., β or m^*_{opt}), but could be naturally explained by the increasing influence of the steep carrier distributions and the failure of the homogeneous reflectivity model. This is also evidenced by the dash-dotted curve in Fig. 3. This curve has been derived from the simulated reflectivity (solid curve in Fig. 6) by applying the same procedure that was used to obtain $N_{e\text{-}h}/(m^*_{opt}F)$ from the experimental reflectivity data (open circles in Fig. 3). The dash-dotted curve reproduces quite well the deviation from the expected linear behavior at higher fluences, demonstrating the increasing importance of the spatial inhomogeneity of the carrier distributions.

It is necessary to make some comments on the influence of band-gap-shrinkage and state and band filling on the results of our calculations. These effects should lead to an increase of both the real and imaginary parts of the dielectric function with carrier density and thus with fluence F. The increase of the imaginary part affects the determination of β (α becomes an increasing function in F). Therefore, the analysis based on Eq. (9) and a pure Drude model (in conjunction with the Fresnel formula) tends to overestimate β. This overestimate is partially canceled by the increase of the real part of the dielectric function, because it shifts the plasma resonance to higher densities. The value of β used in the simulation including all effects (state and band filling, band-gap shrinkage) is therefore only slightly smaller (45 cm/GW) than the value of 50 cm/GW directly obtained from the data. A pure but inhomogeneous Drude-model gives a similar good approximation of our reflectivity data with $\beta = 50$ cm/GW. The differences are within the experimental errors.

The spatial variation of the carrier density also influences the determination of the absolute carrier density shown in Fig. 4. The data points correspond to the directly determined density using a homogeneous reflectivity model (Fresnel formula). Such a description *underestimates* the carrier density at the sample surface. The solid line is taken from our simulations used to fit the measured reflectivity, and should be closer to the true maximum carrier density at the surface.

D. Drude parameter

It is quite remarkable that the Drude model with constant parameters m^*_{opt} and τ_D provides such a good approximation of the measured reflectivity. As discussed in Sec. III C, it is expected that the optical mass increases with carrier density.[12,13] An increase of m^*_{opt} should lead to a strong deviation from the observed linear behavior of $N_{e\text{-}h}/(m^*_{opt}F_0)$. Using the results of our simulations in conjunction with a density-dependent optical mass,[13] the dotted curve in Fig. 3 is calculated from Eq. (9). It is obvious that this curve cannot describe the data. To be consistent with the data, an increasing optical mass would require additional carrier generation mechanisms at high carrier densities. For example, β should double for electron-hole densities around 10^{22} cm^{-3}. Such an increase is unlikely, not only because of state-filling effects which bleach two-photon transitions between the valence and conduction bands. Moreover, from the measured dispersion of β,[33] it is expected that the TPA coefficient should also decrease due to band-gap shrinkage. Another possibility might be impact ionization due to the high plasma temperature, but it is difficult to assess the importance of this effect. To obtain a reasonable estimate of the rate of impact ionization it is necessary to know how the Coulomb interaction between the carriers is screened at high densities. Unfortunately, no experimental data are available for high-density plasmas, and different theoretical viewpoints can be found in the literature.[11,59] A simple static screening model[11] suggests that impact ionization should be negligible. On the

other hand, assuming an unscreened interaction, the impact ionization rate would become comparable to the TPA rate at higher excitation levels. Therefore, the experimentally obtained electron-hole densities shown in Fig. 4 must be regarded as a *lower* limit.

As mentioned before, the experimentally determined Drude damping time of approximately 1 fs is in agreement with both previous high-density experiments[5,31] and theoretical predictions.[52,53] The theoretical studies showed that at high densities electron-hole collisions are responsible for the rather strong damping. In this theoretical work, it has been recognized that the value of $\tau_D = 0.3$ fs, which was obtained by Hulin *et al.*[31] from the analysis of self-reflectivity data, is too high, even for *e-h* scattering. Based on the results presented here we propose an explanation of this discrepancy. In Ref. 31 an inhomogeneous model for carrier generation and reflectivity was used, but two-photon absorption was neglected. For a self-reflectivity measurement the influence of TPA is twofold. TPA creates much steeper carrier distributions than linear and free-carrier absorption alone. Neglecting TPA must then be compensated for by an increased free-carrier absorption, e.g., stronger damping. At $\Delta t = 0$ an additional effect occurs due to the transient increase of the imaginary part of the dielectric function caused by TPA. Again, an apparently higher value of the damping constant is deduced, if the reflectivity data are interpreted *without* TPA.

V. SUMMARY AND CONCLUSIONS

In summary, we have presented a detailed study of the generation and the properties of extremely dense electron-hole plasmas in femtosecond photoexcited silicon. The measured time-resolved reflectivity data can be explained by the Drude-like optical response of the free-carrier plasma, in agreement with simple theoretical considerations. State and band filling and also band-gap shrinkage are of minor importance only.

Based on a careful analysis of the reflectivity data, a lower limit for the plasma density as a function of excitation fluence was determined. The maximum densities were found to be in excess of 10^{22} cm^{-3}, which corresponds to approximately 10% of the total valence-band population. Although a number of studies gave evidence that such high carrier concentrations are created, quantitative values could not be obtained, because of the uncertainties of other physical parameters involved.

Using a simple but surprisingly successful Drude description, we were able to determine important quantities to understand carrier generation in silicon and the optical properties of dense electron-hole plasmas. Within the Drude model an effective two-photon absorption coefficient of $\beta = 50 \pm 10$ cm/GW, an optical mass of $m^*_{opt} = 0.18$, and a Drude damping time of $\tau_D = 1.1$ fs were determined. Free-carrier generation in silicon at higher intensity is therefore dominated by nonlinear absorption. The observed damping time of approximately 1 fs is in agreement with theoretical predictions. An apparently constant value for the optical mass up to very high densities seems to indicate that additional carrier generation mechanisms become important at high fluences.

Moreover, it was demonstrated that the spatial variation of the carrier density and of the optical properties, caused by strong two-photon and free-carrier absorption, must be taken into account. Otherwise, misinterpretation of the experimental data and a drastic underestimate of the carrier density at higher fluences will occur.

Finally, we would like to comment on the relevance of our results in the context of nonthermal laser-induced melting of semiconductors. It is generally accepted that such nonthermal mechanisms are only important above a certain level of electronic excitation of the material: As mentioned in Sec. I, theoretical work[25–29] has set a lower *e-h* density limit of approximately 10^{22} cm^{-3}. To our knowledge, Fig. 4 represents the first explicit quantitative determination of electron-hole densities well in excess of this threshold value. Therefore, the careful characterization of the properties of the strongly excited solid quantitatively supports the models of a plasma-induced lattice instability as an explanation for disordering and melting on a subpicosecond time scale.

ACKNOWLEDGMENTS

K. S-T. gratefully acknowledges support by the *Flughafen Frankfurt Main* foundation. The authors would like to thank J. Bialkowski for assistance with the femtosecond dye laser, and A. Cavalleri for useful discussions and a careful reading of the manuscript.

[1] See, for example, *Proceedings of the 9th International Conference on Hot Carriers in Semiconductors*, edited by K. Hess, J. P. Leburton, and U. Ravaioli (Plenum, New York, 1996), and previous proceedings of this conference.

[2] I. B. Khaibulli, E. I. Shtyrkov, M. M. Zaripov, R. M. Bayazitov, and M. F. Galjantdinov, Radiat. Eff. **36**, 225 (1979).

[3] J. A. Van Vechten, R. Tsu, and F. W. Saris, Phys. Lett. **74A**, 422 (1979).

[4] For a review, see, S. A. Akhmanov, N. I. Koroteev, and I. L. Shumay, *Nonlinear Optical Diagnostics of Laser-Excited Semiconductor Surfaces*, Laser Science and Technology Vol. 2 (Harwood Academic, Chur, 1989).

[5] H. Kurz and N. Bloembergen, in *Energy Beam-Solid Interactions and Transient Thermal Processing*, edited by D. K. Biegelsen, G. A. Rozganyi, and C. V. Shank, MRS Symposia Proceedings No. 35 (Materials Research Society, Pittsburgh, 1985), p. 3, and references therein.

[6] J. M. Liu, A. M. Malvezzi, and N. Bloembergen, Appl. Phys. Lett. **49**, 622 (1986).

[7] M. I. Gallant and H. M. van Driel, Phys. Rev. B **26**, 2133 (1982); J. S. Preston and H. M. van Driel, *ibid.* **30**, 1950 (1984).

[8] H. M. van Driel, Phys. Rev. B **35**, 8166 (1987).

[9] P. M. Fauchet and W. L. Nigham, Jr., Appl. Phys. Lett. **48**, 721 (1986).

[10] D. von der Linde and N. Fabricius, Appl. Phys. Lett. **41**, 991 (1982).

[11] E. J. Yoffa, Phys. Rev. B **21**, 2415 (1980).
[12] H. M. van Driel, Appl. Phys. Lett. **44**, 617 (1984).
[13] G.-Z. Yang and N. Bloembergen, IEEE J. Quantum Electron. **22**, 195 (1986).
[14] M. Rasolt and H. Kurz, Phys. Rev. Lett. **54**, 722 (1985); M. Rasolt, Phys. Rev. B **33**, 1166 (1986).
[15] See, for example, D. von der Linde, in *Resonances—A Volume in Honor of the 70th Birthday of Nicolaas Bloembergen*, edited by M. D. Levenson, E. Mazur, P. S. Pershan, and Y. R. Shen (World Scientific, Singapore, 1990), and references therein.
[16] C. V. Shank, R. Yen, and C. Hirlimann, Phys. Rev. Lett. **50**, 454 (1983); **51**, 900 (1983).
[17] H. W. K. Tom, G. D. Aumiller, and C. H. Brito-Cruz, Phys. Rev. Lett. **60**, 1438 (1988).
[18] K. Sokolowski-Tinten, J. Bialkowski, and D. von der Linde, Phys. Rev. B **51**, 14 186 (1995).
[19] S. V. Govorkov, I. L. Shumay, W. Rudolph, and T. Schröder, Opt. Lett. **16**, 1013 (1991); S. V. Govorkov, T. Schröder, I. L. Shumay, and P. Heist, Phys. Rev. B **46**, 6864 (1992).
[20] P. Saeta, J.-K. Wang, Y. Siegal, N. Bloembergen, and E. Mazur, Phys. Rev. Lett. **67**, 1023 (1991); Y. Siegal, E. N. Glezer, and E. Mazur, Phys. Rev. B **49**, 16 403 (1994); E. N. Glezer, Y. Siegal, L. Huang, and E. Mazur, *ibid.* **51**, 6959 (1995); **51**, 9589 (1995); L. Huang, J. P. Callan, E. N. Glezer, and E. Mazur, Phys. Rev. Lett. **80**, 185 (1998).
[21] K. Sokolowski-Tinten, H. Schulz, J. Bialkowski, and D. von der Linde, Appl. Phys. A: Solids Surf. **53**, 227 (1991).
[22] I. L. Shumay and U. Höfer, Phys. Rev. B **53**, 15 878 (1996).
[23] D. H. Reitze, X. Wang, H. Ahn, and M. C. Downer, Phys. Rev. B **40**, 11 986 (1989); D. H. Reitze, H. Ahn, and M. C. Downer, *ibid.* **45**, 2677 (1992).
[24] V. Heine and J. A. Van Vechten, Phys. Rev. B **13**, 1622 (1976).
[25] R. Biswas and V. Ambegaokar, Phys. Rev. B **26**, 1980 (1982).
[26] Yu. V. Kopaev, V. V. Menyailenko, and S. N. Molotkov, Fiz. Tverd. Tela (Leningrad) **27**, 3288 (1985) [Sov. Phys. Solid State **27**, 1979 (1985)].
[27] P. Stampfli and K. H. Bennemann, Phys. Rev. B **42**, 7163 (1990); Prog. Surf. Sci. **35**, 161 (1991); Phys. Rev. B **46**, 10 686 (1992); **49**, 7299 (1994).
[28] S. Das Sarma and J. R. Senna, Phys. Rev. B **49**, 2443 (1994).
[29] P. L. Silvestrelli, A. Alavi, M. Parrinello, and D. Frenkel, Phys. Rev. Lett. **77**, 3149 (1996).
[30] M. Combescot and J. Bok, J. Lumin. **30**, 1 (1985).
[31] D. Hulin, M. Combescot, J. Bok, A. Migus, J. Y. Vinet, and A. Antonetti, Phys. Rev. Lett. **52**, 1998 (1984).
[32] W. Kütt, A. Esser, K. Seibert, U. Lemmer, and H. Kurz, Proc. SPIE **1268**, 154 (1990).
[33] D. H. Reitze, T. R. Zhang, Wm. M. Wood, and M. C. Downer, J. Opt. Soc. Am. B **7**, 84 (1990).
[34] We did not find any dependence of our data on the orientation of our single-crystalline samples. Therefore, the orientation of the wafers is not specified in the text.
[35] W. Z. Lin, R. W. Schoenlein, J. G. Fujimoto, and E. P. Ippen, IEEE J. Quantum Electron. **24**, 267 (1988).
[36] T. Elsaesser, J. Shah, L. Rota, and P. Lugli, Phys. Rev. Lett. **66**, 1757 (1991).
[37] From the known density of states of silicon in the valence and conduction bands (Ref. 38) a quasi-Fermi energy of the electrons and holes of approximately 1 eV is estimated at a plasma density of 10^{22} cm^{-3}.
[38] M. L. Cohen and J. R. Chelikowski, *Electronic Structure and Optical Properties of Semiconductors* (Springer, Berlin, 1989).
[39] J.-L. Oudar, D. Hulin, A. Migus, A. Antonetti, and F. Alexandre, Phys. Rev. Lett. **55**, 2074 (1985).
[40] J. Shah, R. F. Leheny, and C. Lin, Solid State Commun. **18**, 1035 (1976).
[41] P. A. Wolff, Phys. Rev. **126**, 405 (1962).
[42] *Handbook of Optical Constants of Solids*, edited by E. D. Palik (Academic, Orlando, 1985); G. E. Jellison, Jr., Opt. Mater. **1**, 41 (1992).
[43] R. A. Abraham, G. N. Childs, and P. A. Saunderson, J. Phys. C **17**, 6105 (1984).
[44] A. Oschlies, R. W. Godby, and R. J. Needs, Phys. Rev. B **45**, 13 741 (1992).
[45] R. Zimmermann, Phys. Status Solidi B **146**, 371 (1988).
[46] D. H. Kim, H. Ehrenreich, and E. Runge, Solid State Commun. **89**, 119 (1995).
[47] P. Grosse, *Freie Elektronen in Festkörpern* (Springer, Berlin, 1979).
[48] From standard textbooks (Ref. 49), $m_e^{*-1}=\frac{1}{3}[(2/m_t)+(1/m_l)]$, where m_t is the transverse electron mass, and m_l is the longitudinal electron mass; and $m_h^{*-1}=(m_{lh}^{1/2}+m_{hh}^{1/2})/(m_{lh}^{3/2}+m_{hh}^{3/2})$, where m_{lh} is the light-hole mass and m_{hh} is the heavy-hole mass.
[49] See, for example, S. Wang, *Solid-State Electronics* (McGraw-Hill, New York, 1966).
[50] *Semiconductors: Physics of Group IV Elements and III-V Compounds*, edited by O. Madelung, Landolt-Börnstein, New Series, Group III: Crystal and Solid Stste Physics, Vol. 17 Semiconductors, Pt. a (Springer, Berlin, 1982).
[51] F. Wooten, *Optical Properties of Solids* (Academic, New York, 1972).
[52] M. Combescot, Solid State Commun. **62**, 587 (1987); M. Combescot and R. Combescot, Phys. Rev. B **35**, 7986 (1987).
[53] B. E. Sernelius, Phys. Rev. B **40**, 12 438 (1989); **43**, 7136 (1991).
[54] Using the known temperature dependence of the optical constants of silicon (Ref. 55) an increase of the reflectivity of 7% is expected under our experimental conditions for a temperature of 1685°.
[55] G. E. Jellison, Jr. and H. H. Burke, J. Appl. Phys. **60**, 841 (1986); G. E. Jellison, Jr. and F. A. Modine, Appl. Phys. Lett. **41**, 180 (1982).
[56] K. Sokolowski-Tinten, J. Bialkowski, M. Boing, A. Cavalleri, and D. von der Linde, Phys. Rev. B **58**, R11 805 (1998).
[57] Previous studies of high density *e-h* plasmas in silicon (Refs. 30 and 31) have used self-reflectivity data (which correspond to $\Delta t=0$ fs) to obtain information on plasma generation and plasma properties. Therefore, it may seem inconsistent to assume here a constant value of the reflectivity to integrate Eq. (7). This is not the case for two reasons: (1) The maximum fluence in Refs. 30 and 31 was significantly higher than in this work, resulting in larger changes of the time-averaged reflectivity experienced by the pump pulse. (2) Assuming a constant reflectivity mainly affects the *amount* of laser energy coupled into the material [given by the factor $(1-R)$], and to a much lesser extent *how* it is absorbed inside the sample. The maximum error in $(1-R)$ by assuming $R\approx$const is just a few percent because $\Delta R/R<10\%$.
[58] See, for example, M. Born and E. Wolf, *Principles of Optics* (Pergamon, Oxford, 1980).
[59] V. N. Abakumov, V. I. Perel, and I. N. Yassievich, *Nonradiative Recombination in Semiconductors* (North-Holland, Amsterdam, 1991), Chap. 11.